THE JOURNAL OF PHYSICAL CHEMISTRY A
A JOURNAL OF THE AMERICAN CHEMICAL SOCIETY

pubs.acs.org/JPCA

Article

Correlation between Noncovalent Bond Strength and Spectroscopic Perturbations within the Lewis Base

Steve Scheiner,* Mariusz Michalczyk,* and Wiktor Zierkiewicz

Cite This: *J. Phys. Chem. A* 2024, 128, 10875−10883

Read Online

ACCESS | Metrics & More | Article Recommendations | Supporting Information

ABSTRACT: Me_2CO was allowed to interact with 20 different Lewis acids so as to engage in various sorts of noncovalent interactions, encompassing hydrogen, halogen, chalcogen, pnictogen, and tetrel bonds. Density functional theory computations evaluated the interaction energy of each dyad, which was compared with spectroscopic, geometric, AIM, and energy decomposition elements so as to elucidate any correlations. The red shift of the C═O stretching frequency, and the changes in the nuclear magnetic resonance shielding of the O and C atoms of acetone, are closely correlated with the interaction energy so can be used to estimate the latter from experimental measurements. The standard AIM measures at the bond critical point, ρ, $\nabla^2\rho$, and V also correlate with the energy, albeit not as well as the spectroscopic parameters. The σ-hole depth on the Lewis acid is not well correlated with the energetics, due in part to the fact that electrostatics in general are not an accurate metric of bond strength.

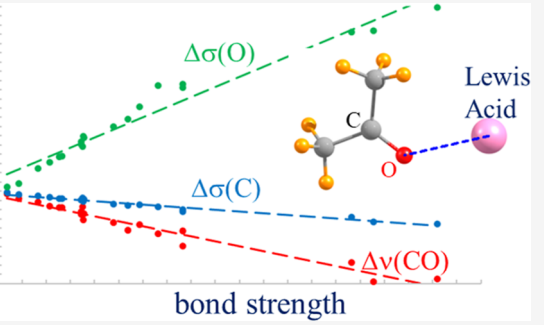

INTRODUCTION

An enormous amount has been learned about the H-bond (HB) in the century since its first appearance in the literature. This phenomenon represents a linchpin in solvation and the structure and function of biological systems.[1−6] The HB is intimately connected in the stability of proteins and the mechanism of numerous enzymes. One of the tools that has proved its value over and over again is spectroscopy. In particular, the shifts in certain infrared (IR) bands or nuclear magnetic resonance (NMR) peaks are frequently interpreted as quantitative measures of the strength of each such bond.[7−9] As one example,[2,10,11] the Badger−Bauer rule relates the red shift of the covalent A−H stretching frequency of the proton donor unit to the strength of the AH···B HB. A similar relationship appears to exist with the downfield shift of the NMR peak of the bridging proton.

Recent years have witnessed a growing recognition of a set of newly rediscovered noncovalent bonds. The proton bridge is replaced by any of a range of different atoms, many ostensibly more electronegative than H. Despite an overall partial negative charge, the electrostatic potential that surrounds this new bridge atom contains a so-called σ-hole, a small positive region that lies along the extension of the covalent bond connecting it to the rest of the molecule. These σ-hole bonds are commonly subdivided based upon the column of the periodic table from which this bridging atom is drawn, as for example the halogen (XB), chalcogen (YB), pnictogen (ZB) or tetrel (TB) bond. In common with its HB parent, this class of bonds[12−36] base their attraction on a Coulombic force, supplemented by charge transfer, polarization, and dispersion. Also like the HB, these bonds are strengthened by electron-withdrawing substituents on the Lewis acid which intensify the σ-hole. They are strengthened as one moves down each column of the periodic table, e.g., Cl < Br < I. First-row atoms, i.e., F, O, N, and C, engage in only weak bonds of this type if at all, but can be coaxed into measurable interactions by appropriate substituents or adding a charge.[37−43]

While research has led to a good deal of fundamental information about these noncovalent bonds, their IR and NMR spectral manifestations have garnered far less attention. The data that has appeared[37,44−59] has been informative to be sure, but does not consider these systems in a systematic manner. As such, there is not now available a thorough understanding of the manner in which each sort of interaction modulates the spectra, nor the processes by which they might do so. Such information would be essential in detecting their presence in a given chemical or biological system. It would also be especially useful if correlations could be established, between certain spectroscopic parameters and the strength or geometry of a given bond, as has proven so very useful for HBs over the years.

Work from this laboratory[40,60−64] has examined this question for a number of types of noncovalent bonds. While a certain degree of correlation has been noted between bond strength and IR and NMR characteristics of the Lewis acid, these correlations are generally too tenuous to serve as a true quantitative yardstick,

Received: October 30, 2024
Revised: November 26, 2024
Accepted: November 30, 2024
Published: December 6, 2024

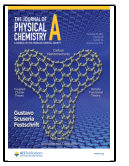

or only apply to a limited subset of molecules. The same weakness of correlation was noted in other measures of bond strength, some of them derived from AIM analysis of the electron density topology.

In contrast to the acid, the relationship does appear to be more robust when comparing bond strength to the spectroscopic properties of the Lewis base unit.[49,64,65] As an early example, based on prior observations,[66,67] one theoretical study[68] paired H_2CO with a number of ions and observed a linear relationship between the interaction energy and the shift of the C═O stretching frequency. More modern investigations have expanded the scope to HBs and their related noncovalent cousins. One study[62] was promising in this respect in that the spectral and other perturbations caused by these sorts of bonds upon a peptide mimic Lewis base seemed to correlate nicely with the bond energy, much better than correlations involving the Lewis acid unit. Another more recent work[69] observed that the change in the stretching frequency of the C═O of a carboxyl group might accurately gauge noncovalent bond strength in certain situations.

The current study is thus aimed to further explore the potential ability of the spectroscopic changes in the Lewis base unit caused by noncovalent bond formation to act as a reliable and accurate probe of bond strength. The prior analysis of the IR spectra of the amide unit[62] involved the amide O as electron donor atom. However, analysis of the spectrum was complicated by the intimate coupling of the C═O stretching motion with that of C−N, into the well-known amide I and II stretching modes. A similar complication relates to the mode mixing within the carboxyl group.[69] In order to more directly focus attention on the carbonyl O which directly donates charge to the Lewis acid, the base chosen for study here is acetone Me_2CO, which contains a much purer C═O stretching mode, and can thus serve as a better model of the carbonyl group in the general case. As a means of broadening the entire picture, a list of 20 different Lewis acid molecules were paired with acetone, covering hydrogen, halogen, chalcogen, pnictogen and tetrel bonds. Substituents that replace H on the pertinent Lewis acids include F, CF_3, and phenyl groups, so as to cover a broad swath of molecular properties. As a further extension, the degree to which the correlations might persist when a given noncovalent bond is weakened by a systematic stretch is assessed so as to offer a window into the occurrence of these bonds within the context of an intramolecular or crystal setting.

METHODS

Full optimizations of isolated monomers and dimers were performed at the M06-2X/def2tzvp level of theory[70−72] using the Gaussian 16 (Rev. C.01) package.[73] Harmonic frequency analysis confirmed their nature as true minima. The counterpoise approach proposed by Boys and Bernardi[74] was implemented to correct the basis set superposition error. The molecular electrostatic potential (MEP) was analyzed to identify the extrema on the 0.001 au electronic isodensity contour of the isolated monomers, utilizing the MultiWFN software.[75,76] Graphical postprocessing of MEP results was performed using the VMD software.[77] Using the AIMAll program,[78] the QTAIM topological analysis[79,80] of the electron density added information about interaction between atoms, represented by bond paths and their bond critical points. NBO analysis[81] identified and quantified the interorbital interactions within dimers and the occupancies of selected orbitals, applying the NBO 7.0 set of codes. Decomposition of interaction energy into its components was achieved in the framework of the ALMO-EDA scheme via Q-Chem 6[82,83] software.

RESULTS AND DISCUSSION

Scheme 1 lays out the set of systems to be considered and the placement of the monomers relative to one another. Each Lewis acid was permitted to approach the O atom of Me_2CO, and the geometry of the dyad fully optimized. The set of Lewis acids listed in Scheme 1 encompassed a variety of different sorts of noncovalent bonds, including hydrogen (HB), halogen (XB), chalcogen (YB), pnictogen (ZB), and tetrel (TB). The atom which interacts directly with the negative regions surrounding the O of acetone contains a positive σ-hole, accounting for a certain amount of electrostatic attraction. The depth of each σ-hole is measured as the maximum of the MEP on a 0.001 au isodensity surface. This quantity is termed V_{max} and is listed in the first column of Table 1 for each of the Lewis acids. There is a large range of this value, varying between 9 and 70 kcal/mol.

Scheme 1. Dimers Examined[a]

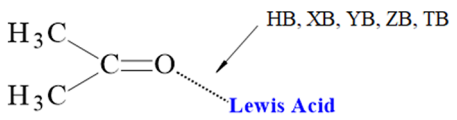

Lewis acids in complexes with acetone

HB	XB	YB	ZB	TB
H_2O	C_6H_5Br	C_6H_5SeF	$C_6H_5AsF_2$	$C_6H_5GeF_3$
CH_4	CF_3Br	SF_2	PF_3	GeF_4
HF	FCl	SeF_4	AsF_3	SnF_4
HCl	FI	TeF_2	SbF_3	PbF_4

[a]Abbreviations: HB-hydrogen bond, XB-halogen bond, YB-chalcogen bond, ZB-pnicogen bond, TB-tetrel bond.

Optimized Dyads. Subsequent to the optimization of each dyad with Me_2CO, a number of properties were elucidated, some of which are reported in Table 1. Just as the σ-hole depths, the interaction energy covers a wide range, varying from less than 1 kcal/mol for the very weak HB with CH_4, up to 36 kcal/mol for the tetrel bond with SnF_4. Formation of each noncovalent bond causes the C═O bond of acetone to lengthen by as much as 0.024 Å in the most extreme cases, as witness the fourth column of Table 1. Also listed in the last two columns are the intermolecular parameters, both the distance between O and the attacking atom of the Lewis acid L, and the angle this bond makes with the C═O axis of acetone. These angles are in the neighborhood of 120°, consistent with a "rabbit ears" view of the two O lone pairs.

In line with the C═O stretching is a red shift of its stretching frequency, as is clear from the first two columns of Table 2. These shifts are roughly proportional to the bond strength, and range up to as high as 98 cm^{-1}. Also of interest from a spectroscopic perspective are the NMR chemical shifts of the C and O atoms of acetone. The calculated shielding of these atoms is listed in Table 2, along with their changes occasioned by the complexation with each Lewis acid. It is clear that the shielding on the C atom diminishes while that of the O center is boosted by the interaction.

The amounts of each shift, whether IR or NMR, closely mirror the noncovalent bond strength. This pattern is clearly depicted

https://doi.org/10.1021/acs.jpca.4c07382
J. Phys. Chem. A 2024, 128, 10875−10883

Table 1. σ-Hole Depth on Lewis Acid Monomer and Characteristics of Optimized Dimers with Me_2CO[a]

dimer	V_{max}	E_{int}	R(C═O)	ΔR(C═O)	R(O···L)	θ(C═O···L)
			HB			
H_2O	44.3	−6.92	1.210	0.006	1.910	114.9
CH_4	8.7	−0.74	1.204	0.001	2.651	119.3
HF	69.7	−11.72	1.213	0.010	1.636	116.9
HCl	45.2	−7.07	1.211	0.007	1.804	120.8
			XB			
C_6H_5Br	9.2	−1.72	1.205	0.002	3.115	102.5
CF_3Br	24.4	−3.33	1.207	0.003	2.921	127.9
FCl	42.0	−7.14	1.209	0.006	2.485	125.8
FI	60.8	−13.27	1.214	0.011	2.548	128.5
			YB			
C_6H_5SeF	28.0	−4.30	1.207	0.003	3.115	95.0
SF_2	35.9	−6.90	1.209	0.006	2.618	122.2
SeF_4	47.5	−10.78	1.213	0.010	2.617	130.4
TeF_2	56.4	−15.29	1.217	0.013	2.533	128.8
			ZB			
$C_6H_5AsF_2$	27.2	−5.09	1.208	0.004	2.908	121.6
PF_3	28.4	−5.33	1.208	0.004	2.812	126.9
AsF_3	40.6	−9.56	1.212	0.008	2.664	128.7
SbF_3	50.0	−15.33	1.217	0.014	2.571	130.9
			TB			
$C_6H_5GeF_3$	36.5	−7.04	1.208	0.004	2.723	127.5
GeF_4	52.6	−29.31	1.224	0.021	2.111	129.3
SnF_4	69.5	−36.36	1.228	0.024	2.210	129.5
PbF_4	70.2	−31.09	1.227	0.023	2.323	127.8

[a] V_{max} and E_{int} in kcal/mol, distances in Å, angles in degrees.

Table 2. C═O Vibrational Frequency (cm^{-1}) and Chemical Shielding (ppm) of C and O Atoms of Me_2CO, and Changes Incurred by Complexation

dimer	ν(C═O)	$\Delta\nu$(C═O)	σ(C)	$\Delta\sigma$(C)	σ(O)	$\Delta\sigma$(O)
acetone	1854		−42.5		−457.4	
			HB			
H_2O	1832	−22	−52.3	−9.8	−403.7	53.7
CH_4	1851	−3	−43.8	−1.3	−452.3	5.0
HF	1818	−36	−57.3	−14.7	−366.0	91.4
HCl	1823	−31	−53.7	−11.1	−398.1	59.3
			XB			
C_6H_5Br	1845	−8	−46.1	−3.6	−449.2	8.2
CF_3Br	1842	−12	−47.2	−4.7	−432.7	24.7
FCl	1829	−24	−51.4	−8.8	−399.4	58.0
FI	1807	−46	−59.5	−16.9	−343.2	114.2
			YB			
C_6H_5SeF	1838	−16	−49.2	−6.7	−425.9	31.4
SF_2	1829	−25	−51.8	−9.2	−407.0	50.4
SeF_4	1812	−42	−58.0	−15.4	−379.3	78.0
TeF_2	1811	−43	−62.6	−20.1	−341.1	116.2
			ZB			
$C_6H_5AsF_2$	1835	−18	−50.6	−8.1	−420.0	37.4
PF_3	1836	−18	−50.3	−7.8	−419.3	38.1
AsF_3	1819	−34	−56.5	−13.9	−387.8	69.6
SbF_3	1795	−59	−64.4	−21.8	−345.4	112.0
			TB			
$C_6H_5GeF_3$	1837	−17	−50.0	−7.5	−409.3	48.1
GeF_4	1777	−77	−71.0	−28.4	−285.0	172.4
SnF_4	1759	−95	−77.7	−35.2	−258.0	199.4
PbF_4	1756	−98	−75.6	−33.0	−283.3	174.1

by the close coincidence between the various points in Figure 1 and the broken line which represents the best linear fit. The R^2 correlation coefficients between E_{int} and $\Delta\nu$(CO), $\Delta\sigma$(C), and $\Delta\sigma$(O) are all equal to 0.96. Each of course has a different slope.

https://doi.org/10.1021/acs.jpca.4c07382
J. Phys. Chem. A 2024, 128, 10875−10883

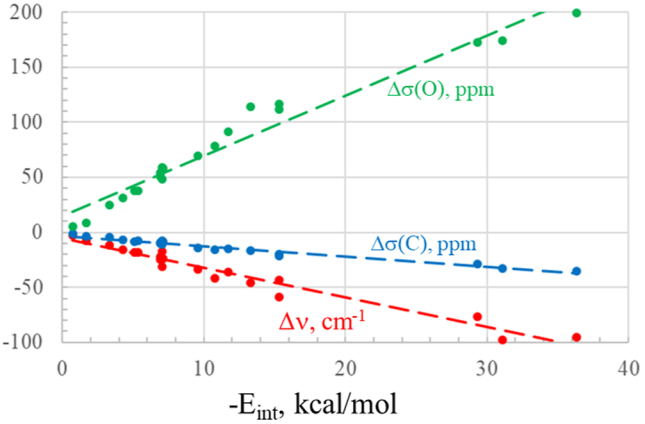

Figure 1. Relationship between interaction energy and spectroscopic measures of noncovalent bond strength.

For example, the O shielding is more sensitive to noncovalent bond formation than is that of C, not unexpected given that it is the former atom that interacts directly with the Lewis acid. For example, an interaction energy of 20 kcal/mol is associated with a 125 ppm increase in the O shielding, while that of C drops by only 20 ppm. The corresponding red shift of the C═O stretching frequency is 60 cm^{-1}. But importantly, these close proportionalities are highly suggestive that one can arrive at a good estimate of the bonding energy by a measurement of any one of these spectroscopic quantities. It is interesting to note finally that in contrast to the excellent correlation between bond strength and C═O red shift, the intensity of this mode is poorly correlated with E_{int}, with R^2 equal to only 0.51. In fact, this intensity enhancement is also poorly correlated (0.63) with the frequency.

It is common in numerous studies of noncovalent interactions to establish bonding by the presence of a bond path between atoms via AIM interpretation of the electron density topology. The numerical value of certain properties at the bond critical point is frequently taken as a measure of the strength of any such bond. In particular, the most commonly used in this regard are the density ρ at this point, its Laplacian $\nabla^2\rho$, and the total potential energy density V. These quantities are all displayed in Table 3, along with the total kinetic energy G, and the ratio of the two latter quantities in the final column. The relationship between these AIM properties and the interaction energy can be seen in Figure 2 to be very nearly linear. The correlation coefficients for such a linear relationship are equal to 0.82 for ρ, 0.92 for $\nabla^2\rho$, and 0.87 for V. Hence, while the linearity is fairly good, these AIM properties are not as accurate a yardstick of bond energy as are the spectroscopic parameters above, with R^2 = 0.96.

There has been some sentiment expressed in the literature that the value of V is closely related to the noncovalent bond energy.[84−86] For example, the equation $E_{int} = 0.5 \times V$ has been applied to HBs. When both are expressed in the same units, the slope of the V curve in Figure 2 translates to a relationship of $E_{int} = 0.66 \times V$. If one were to extract a similar relationship from the other parameters, they would be $E_{int} = -1.00 \times \rho$ and $E_{int} = -0.27 \times \nabla^2\rho$. Note that these linear relationships encompass not only HBs, but the wider panoply of other noncovalent bonds as well.

In connection with AIM analysis, the full molecular diagrams of each dyad are displayed in Figure S1. It may be noted there that in addition to the noncovalent bond of interest to the acetone O, the AIM protocol draws a bond path in many cases to a methyl H atom. Although this bond is a weak one as judged by the bond critical point density, its presence may be a factor in worsening the correlation between E_{int} and the primary noncovalent bond parameters.

Delving into the fundamental nature of each noncovalent bond can offer clues as to their ultimate origin. The total interaction energy of each bond was deconstructed into its component parts by ALMO-EDA decomposition, which provides electrostatic, dispersion, polarization, and charge transfer as separate attractive elements, all countered by Pauli repulsion. The magnitudes of these components are listed in Table 4, along with their percentage contribution to the total attractive energy. One feature that all of these bonds have in common is the large electrostatic term. ES makes up more than half of the total attraction, although this percentage contribution

Table 3. QTAIM Parameters (au) of Bond Critical Point Connecting O of Me_2CO with Lewis Base

dimer	ρ	$\nabla^2\rho$	V	G	$-G/V$
		HB			
H_2O	0.027	0.089	−0.024	0.023	0.958
CH_4	0.006	0.022	−0.003	0.004	1.333
HF	0.053	0.094	−0.057	0.040	0.702
HCl	0.038	0.086	−0.035	0.028	0.800
		XB			
C_6H_5Br	0.010	0.039	−0.006	0.008	1.333
CF_3Br	0.014	0.057	−0.010	0.012	1.200
FCl	0.029	0.119	−0.026	0.028	1.077
FI	0.034	0.113	−0.032	0.030	0.938
		YB			
C_6H_5SeF	0.010	0.037	−0.006	0.008	1.333
SF_2	0.023	0.084	−0.019	0.020	1.053
SeF_4	0.029	0.087	−0.022	0.022	1.000
TeF_2	0.035	0.103	−0.032	0.029	0.906
		ZB			
$C_6H_5AsF_2$	0.015	0.048	−0.010	0.011	1.100
PF_3	0.016	0.052	−0.011	0.012	1.091
AsF_3	0.023	0.068	−0.017	0.017	1.000
SbF_3	0.032	0.090	−0.027	0.025	0.926
		TB			
$C_6H_5GeF_3$	0.016	0.054	−0.013	0.013	1.000
GeF_4	0.063	0.199	−0.082	0.066	0.805
SnF_4	0.064	0.252	−0.085	0.074	0.871
PbF_4	0.060	0.219	−0.071	0.063	0.887

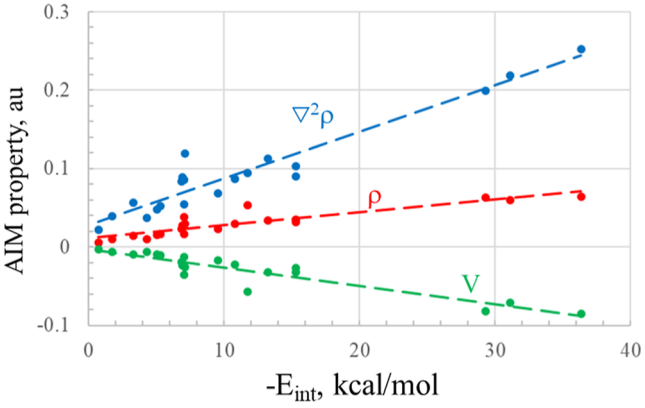

Figure 2. Relationship between interaction energy and AIM measures of noncovalent bond strength at bond critical point.

https://doi.org/10.1021/acs.jpca.4c07382
J. Phys. Chem. A 2024, 128, 10875−10883

Table 4. ALMO-EDA Decomposition of Interaction Energies (kcal/mol)[a]

dimer	ES	%	PAULI	DISP	%	POL	%	CT	%
				HB					
H_2O	−20.00	74	20.05	−3.10	12	−1.71	6	−2.16	8
CH_4	−2.52	66	3.10	−0.98	25	−0.17	4	−0.17	4
HF	−33.78	72	35.36	−3.55	8	−4.13	9	−5.61	12
HCl	−20.66	67	23.78	−3.26	11	−2.67	9	−4.25	14
				XB					
C_6H_5Br	−6.57	63	8.67	−2.81	27	−0.40	4	−0.61	6
CF_3Br	−10.91	72	11.90	−2.58	17	−0.81	5	−0.94	6
FCl	−21.54	66	25.43	−4.17	13	−1.85	6	−5.02	15
FI	−21.21	53	26.50	−6.45	16	−5.19	13	−6.91	17
				YB					
C_6H_5SeF	−11.87	64	14.34	−5.05	27	−0.82	4	−0.91	5
SF_2	−21.93	67	25.68	−5.45	17	−1.82	6	−3.37	10
SeF_4	−32.07	70	35.24	−6.25	14	−3.75	8	−3.98	9
TeF_2	−26.34	55	32.99	−8.29	17	−6.90	14	−6.75	14
				ZB					
$C_6H_5AsF_2$	−17.30	68	20.37	−5.35	21	−1.38	5	−1.39	5
PF_3	−18.13	70	20.58	−4.87	19	−1.40	5	−1.50	6
AsF_3	−29.08	70	31.87	−6.20	15	−3.26	8	−2.86	7
SbF_3	−27.47	57	32.48	−8.27	17	−7.21	15	−4.82	10
				TB					
$C_6H_5GeF_3$	−30.51	73	34.80	−7.14	17	−2.10	5	−2.07	5
GeF_4	−86.21	67	99.32	−10.74	8	−18.85	15	−12.84	10
SnF_4	−56.03	57	61.51	−9.11	9	−19.63	20	−13.09	13
PbF_4	−47.92	56	54.48	−9.05	11	−14.79	17	−13.82	16

[a]ES = electrostatic term, PAULI = Pauli repulsion, DISP = dispersion, POL = polarization, CT = charge transfer. Percentage contributions refer to fraction of sum of attractive elements.

is variable. ES ranges from 53% up to a maximum of 74%. Even more varied are the other three terms. In some cases, it is charge transfer that is the largest of the three, while in others it is dispersion which can account for as much as 27%. There are other cases where polarization energy is larger than either dispersion (DISP) or charge transfer (CT).

Given this variability, it is perhaps not surprising that there is likewise variation in terms of level of correlation with the interaction energy. The polarization energy tracks most closely with E_{int}, with R^2 = 0.97, followed by 0.94 for CT. These correlations are interesting given their small contributions to the total in most cases. The proportionality drops off for the other quantities. R^2 is equal to 0.76 for ES, the largest contributor, and only 0.68 for DISP.

One aspect of the electrostatic energy is associated with the Coulombic attraction between the negatively charged O atom of the acetone and the positive σ-hole of the Lewis acid. Since the correlation between E_{int} and the entire ES component is less than perfect, R^2 = 0.76, it is sensible that the correlation with simply V_{max} is somewhat poorer. As listed in Table 5, which summarizes all of these correlation coefficients, R^2 is equal to only 0.61 for V_{max}.

As there appears to be a strong correlation between polarization and charge transfer and E_{int}, it is instructive to consider another perspective on these quantities. NBO analysis of each of the dyads provides a number of quantitative measures of these phenomena. Table S1 reports the energetic consequence of the transfer of charge from each of the carbonyl O lone pairs to the σ^* antibonding orbital of the Lewis acid, followed by their sum in the last column. These quantities vary from 0.6 to 66 kcal/mol and are roughly proportional to the full interaction energy. A linear relationship between these two properties has a correlation coefficient R^2 equal to 0.91. This correlation is only moderate, and reflects the fact that this charge transfer quantity is only one component of the full interaction energy.

Table 5. Correlation Coefficients Relating Interaction Energy with Indicated Property

property	R^2
$\Delta\nu$(C═O)	0.96
$\Delta\sigma$(C)	0.96
$\Delta\sigma$(O)	0.96
Δr(C═O)	0.98
θ(C═O···L)	0.21
ρ	0.82
$\nabla^2\rho$	0.92
V	0.87
G	0.82
ES	0.76
Pauli	0.75
DISP	0.68
POL	0.97
CT	0.94
V_{max}	0.61
$E(2)$	0.91

Overall, then, the most quantitatively accurate indicators of noncovalent bond energy are the spectroscopic quantities: NMR chemical shifts of O and C, and IR red shift of ν(CO), along with the stretch of the C═O bond. The correlation coefficients of all of these properties exceed 0.96. AIM parameters are in reasonable accord with E_{int}, with R^2 between 0.82 and 0.92; likewise for NBO E2. Within the context of the

https://doi.org/10.1021/acs.jpca.4c07382
J. Phys. Chem. A 2024, 128, 10875−10883

energy components, POL is best (0.97), followed by CT (0.94). The other parameters are in poorer coincidence with E_{int}, despite their larger magnitudes. It is gratifying to note finally the recent observation[69] that stretching frequencies of the C═O group computed by quantum calculations of the sort employed here can provide excellent reproductions of its red shift caused by noncovalent bonding when compared to experimental data, particularly within the context of the M06-2X functional which was applied here.

Geometry Variations. The data discussed above were all extracted from full geometry optimization of each dyad. Such a situation would be most appropriate when each system is free of any external forces that might influence the most favored structure. On the other hand, some of these types of noncovalent bonds may occur in an intramolecular setting, where the two interacting elements are part of an overall molecular backbone that prevents the two components from achieving their desired geometry. Another relevant situation places the bonding species in the solid state, where the geometry between the two species of interest is altered by crystal packing forces.

In an effort to examine how such external forces, and their perturbing effect on the noncovalent bond geometry, influence the various spectroscopic facets, five of the complexes, each representing a different sort of bond, were examined in more detail. The intermolecular distance of each was systematically lengthened in uniform increments. Beginning with the fully optimized structure, the intermolecular distance was stretched by 1.0 Å in 5 increments of 0.2 Å. For each such distance, the intermolecular angle was held as that of the optimized dimer, but the remainder of the geometry was optimized.

The data describing the energetic, geometric, and spectroscopic variations arising from these elongations are contained in Tables S2 and S3. Figure 3 illustrates how these stretches affect

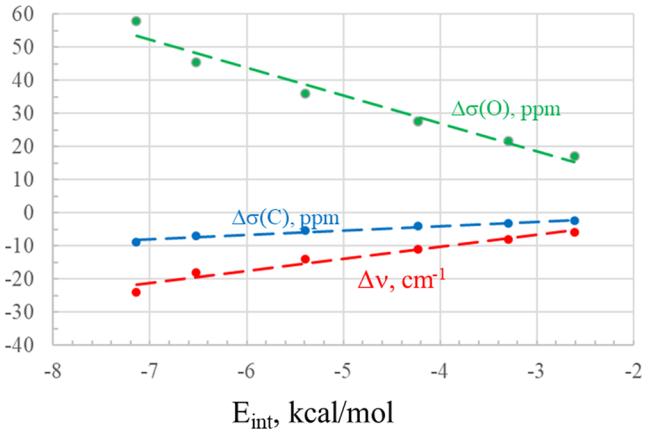

Figure 3. Relationship between interaction energy and spectroscopic measures of halogen bond strength as the FCl molecule is stretched away from the O of acetone.

the energetics and spectroscopic markers of one particular system pairing acetone with FCl in a halogen bond. The horizontal axis refers to the interaction energy, which becomes progressively less negative from left to right as the XB stretches and weakens. The weakening is reflected in a continuous drop of the magnitude of the red shift of the C═O stretching frequency, as indicated by the red curve. Also dropping in magnitude are the shielding increase of O and the decrease of C, the green and blue curves, respectively. Of particular note are the very near linear dependencies of each of these quantities upon the weakening interaction energy. Indeed, the correlation coefficients R^2 for these relationships are all equal to 0.96.

This pattern is not unique to the XB involving FCl. Diagrams akin to Figure 3 were also generated for the other four complexes subject to the same analysis. The corresponding diagrams presented in Figure S2 are remarkably similar to that for the XB, as is the very near linearity of the spectroscopic indicators to the interaction energy. The correlation coefficients are all between 0.93 and 1.00. So one may conclude that the pertinent spectroscopic indices, both IR and NMR, can be used as accurate indicators of bond strength, as external forces stretch and weaken each sort of bond. Not only does this linear relationship apply to five different sorts of noncovalent bond, but also to those of widely varying strength, from 7 to 30 kcal/mol.

CONCLUSIONS

There is a clear and definitive linear relationship between the bond strength and several of the spectral characteristics of the Me_2CO electron donor. This relationship spans a wide gamut of noncovalent interactions, from hydrogen to halogen, chalcogen, pnictogen, and tetrel bonds. Equally diverse is the range of interaction energies, from 1 to as much as 36 kcal/mol. The frequency of the C═O stretching band of H_2CO is red-shifted proportionately to the strength of the bond, such that each 10 cm^{-1} reduction in ν(C═O) signals a bond strengthening of some 3.7 kcal/mol. The NMR shielding of the O nucleus is enhanced by the interaction, rising by 55 ppm for an energy increase of 10 kcal/mol. This same energy rise lowers the C shielding, but by a somewhat lesser amount, of 10 ppm. AIM measures of bond strength are highly accurate, closely correlated with interaction energies for the full set of different bond types. These close relationships persist as the various bonds are weakened by stretching the two units apart, so would be useful when considering intramolecular bonds, and those occurring within crystals. The reader should, however, exercise due caution in applying the principles extracted here from calculations of isolated dimers to systems enmeshed in a crystal where other interactions and crystal packing effects might weaken and even obscure the expected correlations.[87]

ASSOCIATED CONTENT

Supporting Information

The Supporting Information is available free of charge at https://pubs.acs.org/doi/10.1021/acs.jpca.4c07382.

AIM diagrams, data concerning bond stretches, and Cartesian coordinates of complexes (PDF)

AUTHOR INFORMATION

Corresponding Authors

Steve Scheiner − *Department of Chemistry and Biochemistry, Utah State University, Logan, Utah 84322-0300, United States;* orcid.org/0000-0003-0793-0369; Email: steve.scheiner@usu.edu

Mariusz Michalczyk − *Faculty of Chemistry, Wrocław University of Science and Technology, Wrocław 50-370, Poland;* orcid.org/0000-0002-6495-6963; Email: mariusz.michalczyk@pwr.edu.pl

Author

Wiktor Zierkiewicz − *Faculty of Chemistry, Wrocław University of Science and Technology, Wrocław 50-370, Poland;* orcid.org/0000-0002-4038-5959

Complete contact information is available at:
https://pubs.acs.org/10.1021/acs.jpca.4c07382

Notes

The authors declare no competing financial interest.

■ ACKNOWLEDGMENTS

The authors gratefully acknowledge Polish high-performance computing infrastructure PLGrid (HPC Centers: ACK Cyfronet AGH) for providing computer facilities and support within computational grant no. PLG/2023/016853, Wrocław Center for Networking and Supercomputing (WCSS). This material is also based upon work supported by the U.S. National Science Foundation under grant no. 1954310 to S.S. This work was financed in part by a statutory activity subsidy from the Polish Ministry of Science and Higher Education for the Faculty of Chemistry of Wroclaw University of Science and Technology.

■ REFERENCES

(1) Hadzi, D.; Bratos, S. The Hydrogen Bond. In *Recent Developments in Theory and Experiments*, Schuster, P.; Zundel, G.; Sandorfy, C., Eds.; North-Holland Publishing Co.: Amsterdam, 1976; Vol. 2, pp 565−611.
(2) Schuster, P.; Zundel, G.; Sandorfy, C. The Hydrogen Bond. *Recent Developments in Theory and Experiments*; North-Holland Publishing Co.: Amsterdam, 1976.
(3) Scheiner, S.; Wang, L. Hydrogen bonding and proton transfers of the amide group. *J. Am. Chem. Soc.* **1993**, *115*, 1958−1963.
(4) Cuma, M.; Scheiner, S.; Kar, T. Effect of adjoining aromatic ring upon excited state proton transfer. o-Hydroxybenzaldehyde. *J. Mol. Struct.:THEOCHEM* **1999**, *467*, 37−49.
(5) Gilli, G.; Gilli, P. *The Nature of the Hydrogen Bond*; Oxford University Press: Oxford, UK, 2009.
(6) Scheiner, S. *Hydrogen Bonding: A Theoretical Perspective*; Oxford University Press: New York, 1997.
(7) Rivera-Rivera, L. A.; McElmurry, B. A.; Scott, K. W.; Lucchese, R. R.; Bevan, J. W. The Badger−Bauer Rule Revisited: Correlation of Proper Blue Frequency Shifts in the OC Hydrogen Acceptor with Morphed Hydrogen Bond Dissociation Energies in OC−HX (X = F, Cl, Br, I, CN, CCH). *J. Phys. Chem. A* **2013**, *117*, 8477−8483.
(8) Cook, J. L.; Hunter, C. A.; Low, C. M. R.; Perez-Velasco, A.; Vinter, J. G. Solvent effects on hydrogen bonding. *Angew. Chem., Int. Ed. Engl.* **2007**, *46*, 3706−3708.
(9) Du, L.; Mackeprang, K.; Kjaergaard, H. G. Fundamental and overtone vibrational spectroscopy, enthalpy of hydrogen bond formation and equilibrium constant determination of the methanol-dimethylamine complex. *Phys. Chem. Chem. Phys.* **2013**, *15*, 10194−10206.
(10) Boyer, M. A.; Marsalek, O.; Heindel, J. P.; Markland, T. E.; McCoy, A. B.; Xantheas, S. S. Beyond Badger's Rule: The Origins and Generality of the Structure−Spectra Relationship of Aqueous Hydrogen Bonds. *J. Phys. Chem. Lett.* **2019**, *10*, 918−924.
(11) Thatcher, R. J.; Johnson, D. G.; Slattery, J. M.; Douthwaite, R. E. Structure of Amido Pyridinium Betaines: Persistent Intermolecular C−H···N Hydrogen Bonding in Solution. *Chem.—Eur. J.* **2016**, *22*, 3414−3421.
(12) Del Bene, J. E.; Alkorta, I.; Elguero, J. Exploring N···C tetrel and O···S chalcogen bonds in HN(CH)SX:OCS systems, for X = F, NC, Cl, CN, CCH, and H. Chem. *Phys. Lett.* **2019**, *730*, 466−471.
(13) Gougoula, E.; Medcraft, C.; Alkorta, I.; Walker, N. R.; Legon, A. C. A chalcogen-bonded complex H_3NS = C═S formed by ammonia and carbon disulfide characterised by chirped-pulse, broadband microwave spectroscopy. *J. Chem. Phys.* **2019**, *150*, 084307.
(14) Alkorta, I.; Legon, A. An Ab Initio Investigation of the Geometries and Binding Strengths of Tetrel-, Pnictogen-, and Chalcogen-Bonded Complexes of CO_2, N_2O, and CS_2 with Simple Lewis Bases: Some Generalizations. *Molecules* **2018**, *23*, 2250.
(15) Grabowski, S. J. Pnicogen and tetrel bonds—tetrahedral Lewis acid centres. *Struct. Chem.* **2019**, *30*, 1141−1152.
(16) Grabowski, S. Tetrel Bonds with π-Electrons Acting as Lewis Bases—Theoretical Results and Experimental Evidences. *Molecules* **2018**, *23*, 1183.
(17) Alkorta, I.; Elguero, J.; Grabowski, S. J. Pnicogen and hydrogen bonds: complexes between PH_3X^+ and PH_2X systems. *Phys. Chem. Chem. Phys.* **2015**, *17*, 3261−3272.
(18) Franconetti, A.; Quiñonero, D.; Frontera, A.; Resnati, G. Unexpected chalcogen bonds in tetravalent sulfur compounds. *Phys. Chem. Chem. Phys.* **2019**, *21*, 11313−11319.
(19) Franconetti, A.; Frontera, A. Theoretical and Crystallographic Study of Lead(IV) Tetrel Bonding Interactions. *Chem.—Eur. J.* **2019**, *25*, 6007−6013.
(20) Frontera, A.; Bauzá, A. S···Sn Tetrel Bonds in the Activation of Peroxisome Proliferator-Activated Receptors (PPARs) by Organotin Molecules. *Chem.—Eur. J.* **2018**, *24*, 16582−16587.
(21) Murray, J. S.; Politzer, P. σ-Holes and Si···N intramolecular interactions. *J. Mol. Model.* **2019**, *25*, 101.
(22) Clark, T.; Murray, J. S.; Politzer, P. A perspective on quantum mechanics and chemical concepts in describing noncovalent interactions. *Phys. Chem. Chem. Phys.* **2018**, *20*, 30076−30082.
(23) Riley, K. E.; Tran, K.-A. Strength, character, and directionality of halogen bonds involving cationic halogen bond donors. *Faraday Discuss* **2017**, *203*, 47−60.
(24) Riley, K. E.; Vazquez, M.; Umemura, C.; Miller, C.; Tran, K.-A. Exploring the (Very Flat) Potential Energy Landscape of R−Br···π Interactions with Accurate CCSD(T) and SAPT Techniques. *Chem.—Eur. J.* **2016**, *22*, 17690−17695.
(25) Scheiner, S. The pnictogen bond: Its relation to hydrogen, halogen, and other noncovalent bonds. *Acc. Chem. Res.* **2013**, *46*, 280−288.
(26) Zierkiewicz, W.; Michalczyk, M.; Wysokiński, R.; Scheiner, S. On the ability of pnictogen atoms to engage in both σ and π-hole complexes. Heterodimers of $ZF_2C_6H_5$ (Z = P, As, Sb, Bi) and NH_3. *J. Mol. Model.* **2019**, *25*, 152.
(27) Zierkiewicz, W.; Michalczyk, M.; Wysokiński, R.; Scheiner, S. Dual Geometry Schemes in Tetrel Bonds: Complexes between TF_4 (T = Si, Ge, Sn) and Pyridine Derivatives. *Molecules* **2019**, *24*, 376.
(28) Zierkiewicz, W.; Fanfrlík, J.; Michalczyk, M.; Michalska, D.; Hobza, P. S. N chalcogen bonded complexes of carbon disulfide with diazines. Theoretical study. *Chem. Phys.* **2018**, *500*, 37−44.
(29) Dong, W.; Niu, B.; Liu, S.; Cheng, J.; Liu, S.; Li, Q. Comparison of σ-/π-Hole Tetrel Bonds between TH_3F/F_2TO and H_2CX (X = O, S, Se). *ChemPhysChem* **2019**, *20*, 627−635.
(30) Dong, W.; Wang, Y.; Cheng, J.; Yang, X.; Li, Q. Competition between σ-hole pnictogen bond and π-hole tetrel bond in complexes of CF_2=CFZH_2 (Z = P, As, and Sb). *Mol. Phys.* **2019**, *117*, 251−259.
(31) Dong, W.; Li, Q.; Scheiner, S. Comparative Strengths of Tetrel, Pnicogen, Chalcogen, and Halogen Bonds and Contributing Factors. *Molecules* **2018**, *23*, 1681.
(32) Stasyuk, O. A.; Sedlak, R.; Guerra, C. F.; Hobza, P. Comparison of the DFT-SAPT and Canonical EDA Schemes for the Energy Decomposition of Various Types of Noncovalent Interactions. *J. Chem. Theory Comput.* **2018**, *14*, 3440−3450.
(33) Sedlak, R.; Eyrilmez, S. M.; Hobza, P.; Nachtigallova, D. The role of the s-holes in stability of non-bonded chalcogenidebenzene interactions: the ground and excited states. *Phys. Chem. Chem. Phys.* **2018**, *20*, 299−306.
(34) Esrafili, M.; Mousavian, P. Strong Tetrel Bonds: Theoretical Aspects and Experimental Evidence. *Molecules* **2018**, *23*, 2642.
(35) Scheiner, S.; Adhikari, U. Abilities of different electron donors (D) to engage in a PD noncovalent interaction. *J. Phys. Chem. A* **2011**, *115*, 11101−11110.
(36) Esrafili, M. D.; Mousavian, P.; Mohammadian-Sabet, F. Tuning of pnictogen and chalcogen bonds by an aerogen-bonding interaction: a comparative ab initio study. *Mol. Phys.* **2019**, *117*, 58−66.

(37) Del Bene, J. E.; Alkorta, I.; Elguero, J. Anionic complexes of F^- and Cl^- with substituted methanes: Hydrogen, halogen, and tetrel bonds. *Chem. Phys. Lett.* **2016**, *655*−*656*, 115−119.
(38) Scheiner, S. Can two trivalent N atoms engage in a direct NN noncovalent interaction? *Chem. Phys. Lett.* **2011**, *514*, 32−35.
(39) Southern, S. A.; Bryce, D. L. NMR Investigations of Noncovalent Carbon Tetrel Bonds. Computational Assessment and Initial Experimental Observation. *J. Phys. Chem. A* **2015**, *119*, 11891−11899.
(40) Scheiner, S. Comparison of CH···O, SH···O, Chalcogen, and Tetrel Bonds Formed by Neutral and Cationic Sulfur-Containing Compounds. *J. Phys. Chem. A* **2015**, *119*, 9189−9199.
(41) Nziko, V. d. P. N.; Scheiner, S. Comparison of p-hole tetrel bonding with s-hole halogen bonds in complexes of XCN (X = F, Cl, Br, I) and NH_3. *Phys. Chem. Chem. Phys.* **2016**, *18*, 3581−3590.
(42) Liu, M.; Li, Q.; Scheiner, S. Comparison of tetrel bonds in neutral and protonated complexes of pyridineTF_3 and furanTF_3 (T = C, Si, and Ge) with NH_3. *Phys. Chem. Chem. Phys.* **2017**, *19*, 5550−5559.
(43) Scheiner, S. Systematic Elucidation of Factors That Influence the Strength of Tetrel Bonds. *J. Phys. Chem. A* **2017**, *121*, 5561−5568.
(44) Alkorta, I.; Rozas, S.; Elguero, J. Charge-transfer complexes between dihalogen compounds and electron donors. *J. Phys. Chem. A* **1998**, *102*, 9278−9285.
(45) Zhou, Z.-J.; Liu, H.-L.; Huang, X.-R.; Li, Q.-Z.; Sun, C.-C. Effect of substitution and cooperativity on the Cl−F blue shift in single-electron halogen-bonded H3C ··· ClF complex. *Mol. Phys.* **2010**, *108*, 2021−2026.
(46) Wang, W.; Zhang, Y.; Ji, B.; Tian, A. On the correlation between bond-length change and vibrational frequency shift in halogen-bonded complexes. *J. Chem. Phys.* **2011**, *134*, 224303.
(47) Ford, T. A. An ab initio study of some halogen-bonded complexes containing cyclic ethers. *Mol. Phys.* **2021**, *119*, No. e1919326.
(48) Bene, J. E. D.; Alkorta, I.; Elguero, J. Properties of cationic pnictogen-bonded complexes $F_{4-n}H_nP^+$:N-base with H−P···N linear and n = 1−4. *Mol. Phys.* **2016**, *114*, 102−117.
(49) Ellington, T. L.; Reves, P. L.; Simms, B. L.; Wilson, J. L.; Watkins, D. L.; Tschumper, G. S.; Hammer, N. I. Quantifying the Effects of Halogen Bonding by Haloaromatic Donors on the Acceptor Pyrimidine. *ChemPhysChem* **2017**, *18*, 1267−1273.
(50) Esrafili, M. D.; Vakili, M. The effect of hydrogen-bonding cooperativity on the strength and properties of σ-hole interactions: an ab initio study. *Mol. Phys.* **2017**, *115*, 913−924.
(51) Gholipour, A.; Farhadi, S.; Neyband, R. S. Theoretical investigation of the nature and strength of simultaneous interactions of $\pi-\pi$ stacking and halogen bond including NMR, SAPT, AIM and NBO analysis. *Struct. Chem.* **2016**, *27*, 1543−1551.
(52) Cormanich, R. A.; Rittner, R.; O'Hagan, D.; Bühl, M. Inter- and intramolecular CF···C = O interactions on aliphatic and cyclohexane carbonyl derivatives. *J. Comput. Chem.* **2016**, *37*, 25−33.
(53) Viger-Gravel, J.; Leclerc, S.; Korobkov, I.; Bryce, D. L. Correlation between C chemical shifts and the halogen bonding environment in a series of solid para-diiodotetrafluorobenzene complexes. *CrystEngComm* **2013**, *15*, 3168−3177.
(54) Alkorta, I.; Sánchez-Sanz, G.; Elguero, J.; Del Bene, J. E. Influence of hydrogen bonds on the P···P pnictogen bond. *J. Chem. Theory Comput.* **2012**, *8*, 2320−2327.
(55) Ma, N.; Zhang, Y.; Ji, B.; Tian, A.; Wang, W. Structural competition between halogen bonds and lone-pair..p interactions in solution. *ChemPhysChem* **2012**, *13*, 1411−1414.
(56) Ghafari Nikoo Jooneghani, S.; Gholipour, A. Mutual cooperation of π-π stacking and pnictogen bond interactions of substituted monomeric Lawesson's reagent and pyridine rings: Theoretical insight into Pyr∥X-PhPS2⊥pyr complexes. *Chem. Phys. Lett.* **2019**, *721*, 91−98.
(57) Watson, B.; Grounds, O.; Borley, W.; Rosokha, S. V. Resolving the halogen vs. hydrogen bonding dichotomy in solutions: intermolecular complexes of trihalomethanes with halide and pseudohalide anions. *Phys. Chem. Chem. Phys.* **2018**, *20*, 21999−22007.
(58) Xu, Y.; Gabidullin, B.; Bryce, D. L. Single-Crystal NMR Characterization of Halogen Bonds. *J. Phys. Chem. A* **2019**, *123*, 6194−6209.
(59) Parra, R. D.; Grabowski, S. J. Enhancing Effects of the Cyano Group on the C-X···N Hydrogen or Halogen Bond in Complexes of X-Cyanomethanes with Trimethyl Amine: $CH_{3-n}(CN)_nX\cdots NMe_3$, (n = 0−3; X = H, Cl, Br, I). *Int. J. Mol. Sci.* **2022**, *23*, 11289.
(60) Scheiner, S. Ability of IR and NMR Spectral Data to Distinguish between a Tetrel Bond and a Hydrogen Bond. *J. Phys. Chem. A* **2018**, *122*, 7852−7862.
(61) Lu, J.; Scheiner, S. Effects of Halogen, Chalcogen, Pnicogen, and Tetrel Bonds on IR and NMR Spectra. *Molecules* **2019**, *24*, 2822.
(62) Michalczyk, M.; Zierkiewicz, W.; Wysokiński, R.; Scheiner, S. Theoretical Studies of IR and NMR Spectral Changes Induced by Sigma-Hole Hydrogen, Halogen, Chalcogen, Pnicogen, and Tetrel Bonds in a Model Protein Environment. *Molecules* **2019**, *24*, 3329.
(63) Lu, J.; Scheiner, S. Relationships between Bond Strength and Spectroscopic Quantities in H-Bonds and Related Halogen, Chalcogen, and Pnicogen Bonds. *J. Phys. Chem. A* **2020**, *124*, 7716−7725.
(64) Amonov, A.; Scheiner, S. Relation between Halogen Bond Strength and IR and NMR Spectroscopic Markers. *Molecules* **2023**, *28*, 7520.
(65) Attrell, R. J.; Widdifield, C. M.; Korobkov, I.; Bryce, D. L. Weak Halogen Bonding in Solid Haloanilinium Halides Probed Directly via Chlorine-35, Bromine-81, and Iodine-127 NMR Spectroscopy. *Cryst. Growth Des.* **2012**, *12*, 1641−1653.
(66) Bellamy, L. J.; Pace, R. J. Hydrogen bonding in alcohols and phenols. III. Hydrogen bonds between alcohols and carbonyl groups. *Spectrochim. Acta, Part A* **1971**, *27*, 705−713.
(67) Thijs, R.; Zeegers-Huyskens, T. Infrared and Raman studies of hydrogen bonded complexes involving acetone, acetophenone and benzophenone I. Thermodynamic constants and frequency shifts of the n_{OH} and $n_{C=O}$ stretching vibrations. *Spectrochim. Acta, Part A* **1984**, *40*, 307−313.
(68) Latajka, Z.; Scheiner, S. Correlation between interaction energy and shift of the carbonyl stretching frequency. *Chem. Phys. Lett.* **1990**, *174*, 179−184.
(69) Bhattacharya, I.; Banerjee, P. From 'halogen' to 'tetrel' bonds: matrix isolation IR spectroscopic and quantum mechanical studies of the effect of central atom substitution in donor tetrahalogens on binary complex formation with formic acid. *Phys. Chem. Chem. Phys.* **2024**, *26*, 21538−21547.
(70) Weigend, F. Accurate Coulomb-fitting basis sets for H to Rn. *Phys. Chem. Chem. Phys.* **2006**, *8*, 1057−1065.
(71) Zhao, Y.; Truhlar, D. G. Density functionals with broad applicability in chemistry. *Acc. Chem. Res.* **2008**, *41*, 157−167.
(72) Zhao, Y.; Truhlar, D. G. The M06 suite of density functionals for main group thermochemistry, thermochemical kinetics, noncovalent interactions, excited states, and transition elements: two new functionals and systematic testing of four M06-class functionals and 12 other functionals. *Theor. Chem. Acc.* **2008**, *120*, 215−241.
(73) Frisch, M. J.; Trucks, G. W.; Schlegel, H. B.; Scuseria, G. E.; Robb, M. A.; Cheeseman, J. R.; Scalmani, G.; Barone, V.; Petersson, G. A.; Nakatsuji, H.; et al. *Gaussian 16*, Revision C.01; Gaussian, Inc.: Wallingford, CT, 2016.
(74) Boys, S. F.; Bernardi, F. The calculation of small molecular interactions by the differences of separate total energies. Some procedures with reduced errors. *Mol. Phys.* **1970**, *19*, 553−566.
(75) Lu, T.; Chen, F. Quantitative analysis of molecular surface based on improved Marching Tetrahedra algorithm. *J. Mol. Graph. Model.* **2012**, *38*, 314−323.
(76) Lu, T.; Chen, F. Multiwfn A multifunctional wavefunction analyzer. *J. Comput. Chem.* **2012**, *33*, 580−592.
(77) Humphrey, W.; Dalke, A.; Schulten, K. VMD: Visual molecular dynamics. *J. Mol. Graphics* **1996**, *14*, 33−38.
(78) Keith, T. A. *AIMAll*; TK Gristmill Software: Overland Park KS, 2013.
(79) Bader, R. F. W. A Bond Path: A Universal Indicator of Bonded Interactions. *J. Phys. Chem. A* **1998**, *102*, 7314−7323.

https://doi.org/10.1021/acs.jpca.4c07382
J. Phys. Chem. A 2024, 128, 10875−10883

(80) Popelier, P. L. A. *Atoms in Molecules. An Introduction*; Prentice Hall: Harlow, UK, 2000.
(81) Weinhold, F.; Landis, C. R.; Glendening, E. D. What is NBO analysis and how is it useful? *Int. Rev. Phys. Chem.* **2016**, *35*, 399−440.
(82) Horn, P. R.; Mao, Y.; Head-Gordon, M. Probing non-covalent interactions with a second generation energy decomposition analysis using absolutely localized molecular orbitals. *Phys. Chem. Chem. Phys.* **2016**, *18*, 23067−23079.
(83) Horn, P. R.; Mao, Y.; Head-Gordon, M. Defining the contributions of permanent electrostatics, Pauli repulsion, and dispersion in density functional theory calculations of intermolecular interaction energies. *J. Chem. Phys.* **2016**, *144*, 114107.
(84) Espinosa, E.; Molins, E.; Lecomte, C. Hydrogen bond strengths revealed by topological analyses of experimentally observed electron densities. *Chem. Phys. Lett.* **1998**, *285*, 170−173.
(85) Espinosa, E.; Alkorta, I.; Rozas, I.; Elguero, J.; Molins, E. About the evaluation of the local kinetic, potential and total energy densities in closed-shell interactions. *Chem. Phys. Lett.* **2001**, *336*, 457−461.
(86) Mata, I.; Alkorta, I.; Espinosa, E.; Molins, E. Relationships between interaction energy, intermolecular distance and electron density properties in hydrogen bonded complexes under external electric fields. *Chem. Phys. Lett.* **2011**, *507*, 185−189.
(87) Southern, S. A.; West, M. S.; Bradshaw, M. J. Z.; Bryce, D. L. Experimental C and ^{1}H Solid-State NMR Response in Weakly Tetrel-Bonded Methyl Groups. *J. Phys. Chem. C* **2021**, *125*, 2111−2123.

https://doi.org/10.1021/acs.jpca.4c07382
J. Phys. Chem. A 2024, 128, 10875−10883